Journal of Composites and Compounds 6(2024) 1-6

Available Online at www.jourcc.com

Journal homepage: www.JOURCC.com

Journal of Composites and Compounds

Influence of ionic size on the concentration of Ag^+ and Zn^{2+} in simulated body fluid: Modeling and Monte Carlo simulation with dental applications

Masoumeh Khamehchi [a]*, ***Ana Chkhenkeli*** [b]*

[a] *Department of Basic Science, Hamedan University of Technology, P. O. Box: 65169-1-3733, Hamedan, Iran*

[b] *BAU International University, Batumi School of Medicine and Health Science, Georgia*

ABSTRACT

The influences of silver (Ag^+) and zinc (Zn^{2+}) ions, and their proposed action on bioactive glass for dental applications, are investigated through computational modeling and Monte Carlo simulation. Bioactive glass materials will continue to be adopted as dental restorative materials, pulp-capping agents, and implant coatings because they can provide a potentially therapeutic way to deliver ions that may possess antimicrobial properties and help stimulate tissue regeneration. Profiles of Ag^+ and Zn^{2+} as a function of time in simulated body fluid were simulated to compare and contrast their release behavior. Zn^{2+}, having a smaller ionic radius, may be released more efficiently than Ag^+ making Zn^{2+} has a greater release potential while Ag^+ may release more slowly, and some may have been retained even in the bioactive glass structure. Monte Carlo simulation allows for best assessment of the stochastic nature of ion transport that enabled the visualization of release potential and release efficiencies in chronological blocks of information. The findings indicate how important it will be to consider ionic size, transport mechanisms, and release potential when designing bioactive glass. If bioactive glass or bioactive materials can be designed with a target of delivery and duration of release it may be feasible to use Zn^{2+} or Ag^+ to facilitate remineralization, support pulpal healing and long-term antibacterial protection in dental applications while also fostering the advancement of controlled programmable bioactive dental materials.

Peer review under responsibility of UGPH.

ARTICLE INFORMATION

Article History:
Received 05 October 2024
Received in revised form 24 December 2024
Accepted 28 December 2024

Keywords:
Bioactivity
Modeling
Monte Carlo simulation
Ion concentration
Dental application

1. Introduction

Bone injuries are currently one of the most frequent health problems in populations worldwide [1, 2]. Due to the need for regeneration or for replacement of damaged bone tissue, the creation of polymer–inorganic composite biomaterials resembling the composition and architecture of native bone warrants increasing attention [1, 3-7]. Since bioactive glasses (BGs) exhibit biocompatibility and osteoconductivity they represent a prominent group of materials in this respect. Typically comprised of silica (SiO_2), calcium oxide (CaO), phosphorus pentoxide (P_2O_5), and sodium oxide (Na_2O), these glasses represent a system able to bond to bone and stimulate tissue healing [8-13].

Bioactive glasses (BGs) offer strong interfacial bonding with the surrounding host tissue through a series of complex chemical and biochemical interactions. As a result, BGs are desirable candidates for use in multiple clinical applications [14, 15]. Amongst the bioactive glasses previously discussed the development of nanoscale 58S bioactive glass has received much attention as it shoots favorable biological properties, including, in vitro, it has been shown to promote angiogenesis. Numerous methods of synthesis have been utilized in the preparation of nanosized 58S BG including: surfactant-assisted sol-gel [16, 17], co-precipitation [3], conventional sol-gel [18-20], and powder metallurgy [21].

Revision operations for infection-related bioactive glass (BG)-based implants prompt the necessity to enhance the functional characteristics. Antimicrobial properties of various ions have been known for centuries, especially in Mediterranean and Asian societies, to which we refer [24]. More recently, therapeutic ions such as aluminum [22]. More recently, therapeutic ions such as aluminum [23], strontium [24], copper [25, 26], fluoride [27], silver [28], and zinc [29], have been doped into bioactive glass matrices to advance the biological performance of the biomaterial. Silver and zinc have been given more attention due to their antibacterial and anticancer properties. Silver oxide (Ag_2O) has

* *Corresponding authors: Masoumeh Khamehchi & Ana Chkhenkeli, Emails: mkhamehchi@gmail.com, anukachx@gmail.com*

https://doi.org/10.61882/jcc.6.4.5

been widely recognized for its antimicrobial efficacy and notable biological activity [30-33].

In a study by Sharifianjazi et al., it was demonstrated that bioactive glass composed of SiO_2–P_2O_5–CaO–Ag_2O containing 2 mol% Ag_2O exhibited superior bioactivity compared to compositions with 4 and 6 mol% Ag_2O. Notably, the apatite morphology in the 2 mol% sample displayed a dispersed glacier-like structure after 14 days of immersion [28]. In a related investigation, the same research group reported that the highest rate of hydroxyapatite (HA) crystallization occurred in a SiO_2–P_2O_5–CaO–SrO–Ag_2O system with 5 mol% Ag_2O, outperforming other compositions evaluated [33]. Moreover, it was found that lower silver contents (3 and 5 mol% Ag_2O) significantly enhanced the proliferation and osteogenic differentiation of G292 osteoblast-like cells [33]. In another study, Phetnin et al. [34] synthesized materials from the $80SiO_2$–(15−x) CaO–$5P_2O_5$–xAg_2O series (with x ranging from 0 to 5 mol%) for applications in bone regeneration and drug delivery. Their findings confirmed that silver-doped mesoporous bioactive glass microspheres (Ag-MBGMs) exhibited effective antibacterial activity against Staphylococcus aureus and Escherichia coli, indicating strong potential for clinical use.

In parallel, zinc has also emerged as a critical element due to its essential role in bone cell proliferation, DNA replication [35, 36], protein synthesis, and enzymatic function as a cofactor in numerous biological processes [37-40]. Zeeshan fabricated HPMC crosslinked chitosan scaffolds reinforced with bioactive glass for alveolar bone repair. The scaffolds showed improved pore structure (90.5–132 μm) and mechanical strength (0.451 MPa). Cytotoxicity tests confirmed cell viability, while assays demonstrated enhanced pre-osteoblast growth, adhesion, and differentiation. Antibacterial testing revealed a 35% reduction in *S. aureus* viability. These findings indicate Zeeshan's scaffolds are promising for alveolar bone regeneration [35].

Recent studies have focused on enhancing the biological performance of bioactive glasses by incorporating therapeutic ions such as silver and zinc. In Ref. [41], SiO_2-P_2O_5-CaO-xAg_2O and SiO_2–P_2O_5–CaO-*x*ZnO systems (*x* = 2 and 4 mol%) have been synthesized via the sol-gel method to evaluate their bioactivity, cytocompatibility, and antibacterial properties. Among the tested compositions, the glass containing 2 mol% Ag_2O (BA2) demonstrated the highest rate of crystalline HA formation, surpassing both the zinc-substituted and higher silver-content samples. MTT and ALP assays confirmed that this composition also promoted osteoblastic cell proliferation and differentiation. Additionally, antibacterial tests indicated superior antimicrobial activity in Ag-doped glasses compared to their Zn-doped counterparts. These findings suggest that low-level silver incorporation (2 mol%) enhances both the biological and antibacterial performance of bioactive glasses, positioning this composition as a promising candidate for bone tissue engineering applications [41]. Although the incorporation of silver and zinc in bioactive glasses (BGs) has been widely studied, a comprehensive predictive model tailored for BGs containing Ag_2O or ZnO is lacking. Existing models mostly rely on molecular dynamics (MD), with limited use of machine learning (ML) or mathematical approaches. MD simulations have revealed key hydration and ion exchange processes, while ML models have predicted mechanical properties such as elastic modulus based on compositional variations [42]. Despite these efforts, current methods do not fully capture the complexity of ion release.

Mathematical models like those predicting degradation and hydroxyapatite formation offer practical advantages with reduced computational cost. Ion release studies are crucial for understanding the bioactivity, antibacterial effects, and regenerative potential of BGs. Evaluating ion release under varying environmental conditions is essential for developing effective restorative and regenerative materials, as the size of the released ions significantly influences their diffusion rates, bioavailability, and interaction with surrounding tissues [43, 44].

This study investigates how the ionic size of Ag_2O and ZnO influences their release behavior from bioactive materials designed for dental applications. Understanding these size-dependent release dynamics is essential for optimizing therapeutic ion delivery in restorative dentistry, particularly to enhance antimicrobial activity and promote pulp and dentin regeneration. Computational models are presented to simulate ion concentration profiles in simulated body fluid (SBF), and combined with Monte Carlo simulations [45] to assess the probability of effective ion release, and the associated risk as the ion release is contextually put into a clinically-relevant safety threshold. The quantitative analysis is likely to assess the ideal timeframes for the delivery of ions to guide the design of advanced dental materials that rely on manageable release of functional ions, such as restorative cements, pulp-capping agents, and implant coatings.

2. Materials and methods

2.1. Modeling the concentration of silver oxide (Ag_2O) nanoparticles in SBF

To describe the concentration of silver oxide (Ag_2O) nanoparticles in SBF solution, a first-order kinetic uptake model is applied. This model presumes that the release rate of Ag_2O in the surrounding medium is a time-dependent process.

$C(t)$ represents the concentration of Ag_2O (or released Ag^+ ions) in SBF at time *t*, and C_∞ represents the theoretical maximum (equilibrium) concentration achievable in the experimental conditions (i.e., maximum solution concentration). The rate of concentration can be described by the first-order differential equation:

$$\frac{dC(t)}{dt} = k(C_\infty - C(t)) \quad (1)$$

Where *k* is a constant. This equation captures the fact that the release rate is initially rapid when the system is far from equilibrium, and progressively slows down as the concentration approaches C_∞. By separating variables and integrating, it is obtained that:

$$C(t) = C_\infty(1 - e^{-kt}) \quad (2)$$

2.2. Modeling the concentration of zinc oxide (ZnO) nanoparticles in SBF

To evaluate the temporal evolution of ZnO concentration in SBF, a first-order decay model is employed. This model is suitable when the concentration of a species decreases exponentially over time due to mechanisms such as adsorption, precipitation, or re-uptake by a surface. The model assumes that the rate of decrease in Zn^{2+} concentration is proportional to its instantaneous concentration in solution:

$$\frac{dC'(t)}{dt} = k'C'(t) \quad (3)$$

Where $C'(t)$ is the ZnO concentration at time *t*. k' is the constant. Solving the differential equation, it is obtained that:

$$C'(t) = C_0 e^{-k't} \quad (4)$$

Where C_0 is a constant.

2.3. Success probability: The probability of meeting design specifications

Experimentally determined parameters k, k', C_0, and C_∞ inherently contain uncertainty due to measurement noise, sample variability, and model fitting limitations. To quantitatively assess the impact of these uncertainties on the model's predictive capacity, Monte Carlo simulation techniques are employed. Parameters k, k', C_0, and C_∞ from probabilistic distributions derived from their estimated confidence intervals. By integrating the Monte Carlo method with the models presented in Sec. 2.1 and Sec. 2.2 A robust framework for understanding how time affects the probability of successful performance, defined as the system remaining within its designated safe and functional limits.

3. Results and discussion

3.1. Modeling and validation

The mathematical models described in Sections 2.1 and 2.2 are employed to predict 4 mol% Ag_2O and 4 mol% ZnO concentrations. For this purpose, the experimental data provided by Shahrbabak et al. [41] is divided into two subsets: a training set and a test set. The training set is utilized to estimate the unknown parameters in Eqs. (2) and (4), while the test set serves to validate the model's predictive accuracy. The chemical composition of Ag-BG with 4 mol% Ag_2O, labeled by BA4, and Zn-BG with 4 mol% ZnO, labeled by BA4, is detailed in Table 1.

Table. 1.
The chemical composition of Ag-BG and Zn-BG (mol%) [28, 41].

Sample	SiO_2	P_2O_5	CaO	Ag_2O	ZnO
BZ4	60	4	36	0	4
BA4	60	4	36	4	0

Using the training dataset, the unknown parameters in Eqs. (2) and (4) are determined from the experimental data as outlined below:

$$C(t) = 0.39(1 - e^{-1.13t}) \quad (5)$$

$$C'(t) = 9.31e^{-0.19\,t} \quad (6)$$

Fig. 1 presents a comparison between the predicted and experimental concentrations of BZ4 and BA4, immersed in SBF at various time intervals. The results show strong agreement between the model predictions and the experimental observations, indicating that the developed model accurately estimates the release of Ag and Zn with overall coefficients of variation of 0.95%, 7%, respectively, when compared to the test dataset [41]. The ion concentration of Ag can be compared to the ion concentration of Zn in SBF (see Fig. 2). The concentration of Zn ions is higher than that of Ag ions. The reason Zn ions are much higher concentration in SBF compared to Ag can be explained by ionic size. Zn ions with smaller ionic sizes are able to diffuse through the glass structure and into the surrounding solution easier than Ag with its larger ionic size, which is limited in diffusion, and also potentially retained more in the glass matrix structure; the smaller ionic size of Zn is able to break the glass matrix more easily encouraging dissolution and availability of the ions into surrounding medium more readily. Overall, the difference in size between the Zn and Ag would influence their release. In more detail, the smaller the ionic size of Zn^{2+} made it more mobile and weakly retained in the glass matrix lessening its diffusion limitations and increasing dissolution abilities into SBF. The larger Ag^{+} ion constitutes diffusion restrictions, and its precipitation further limited the total concentration in solution. Therefore, the difference in ionic size could account for the observation made in their respective release behaviors.

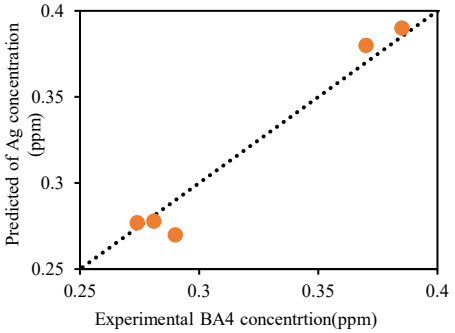

(a)

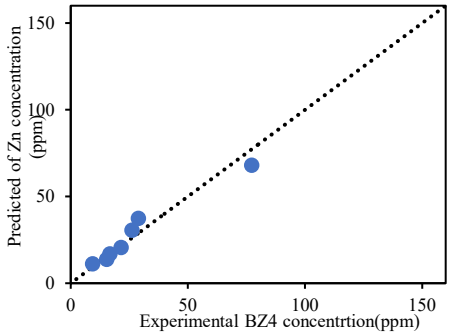

(b)

Fig. 1. Comparison of predicted values of concentrations of elements (a) Ag, (b) Zn in the SBF solution with soaking time for silicon [41].

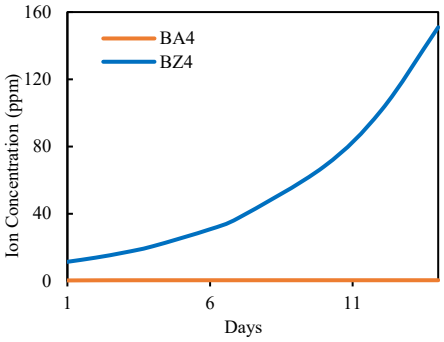

Fig. 2. Comparison of concentrations of Ag with Zn in the SBF solution with soaking time for silicon.

3.2. Success probability: The probability of meeting design specifications for BA4 and BZ4

In this study, the experimental data reported by Shahrbabak et al. [41] are used to establish the limit state functions (*LSFs*). Based on the ion release concentrations of BA4 and BZ4, the *LSF*s are defined as follows:

$$\dot{c}_{Ag_2O} < 0.03 \quad (7)$$

$$\dot{c}_{ZnO} < 3 \quad (8)$$

Here, $\dot{C}_{Ag_2O}$ and $\dot{C}_{ZnO}$ represent the time derivatives of the ion release concentrations of Ag_2O and ZnO, respectively. These

thresholds are derived directly from the experimental observations reported in [41]. Normal probability distributions are assumed for experimentally determined parameters k, k', C_0, and C_∞. The specified Characteristics for these parameters are detailed in Table 2. To evaluate the success probability, 100,000 random samples are generated for each parameter within its respective ranges. These samples are used to calculate the probability that the photovoltaic outputs fall within the predefined functional safety region, as determined by the developed model.

Table 2
Parameter ranges applied in the Monte Carlo simulation, adapted from Shahrbabak et al. [41].

Parameters	Mean (μ)	Std. Dev. (σ)
k	1.13	0.05
k'	0.19	0.02
C_0	9.31	0.47
C_∞	0.39	0.05

Fig. 3 presents the computed success probabilities of the time derivative of Ag_2O ion concentration as a function of time. The circular markers represent data obtained from Monte Carlo simulations, while the overlaid polynomial regression curves are fitted to these data points. In the regression equations, y denotes the success probability and x represents time. The figure displays the probability that the rate of Ag_2O ion release ($\dot{C}_{Ag_2O}$) falls below 0.03 over 14 days, based on Monte Carlo simulations. For the first 9 days, the probability remains near 0%, indicating a very low probability, which suggests that the release rate remains above the threshold during this early phase. Starting from day 10, the probability begins to increase, reaching about 80% by day 14, signaling a noticeable decrease in the Ag_2O release rate late in the period. This behavior reflects a delayed but accelerating reduction in ion release, likely due to the larger ionic size of Ag^+ and its stronger interaction with the glass matrix. The fitted polynomial curve (with an R^2 = 0.9999) provides an excellent match to the simulation data, making it a reliable model for describing and predicting Ag^+ ion release behavior over time.

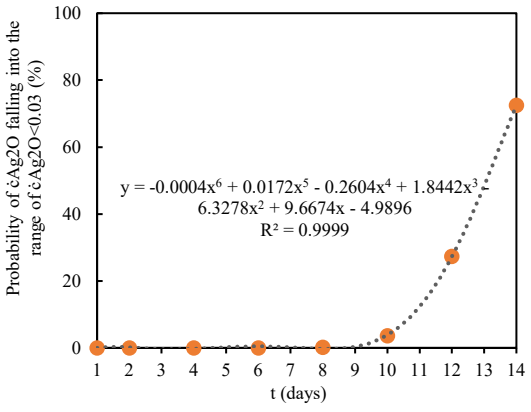

Fig. 3. The success probability of time derivation of Ag_2O concentration release in terms of time.

Fig. 4 shows the calculated success probabilities of the time derivative of ZnO ion concentration over time. The circular markers indicate data generated through Monte Carlo simulations, while the superimposed polynomial regression curves are fitted to these points. In the regression equations, y represents the success probability, and x corresponds to time. The figure shows the probability that the rate of ZnO ion release ($\dot{C}_{ZnO}$) falls below 1 over 14 days, based on Monte Carlo simulations. Initially near 0%, the probability rises sharply to nearly 100% by day 5, indicating a rapid early release followed by a significant slowdown. This plateau suggests that Zn^{2+} ions diffuse quickly at first, then stabilize as the glass matrix depletes. The fitted 6th-degree polynomial (R^2 = 0.9929) accurately models this behavior, reflecting a typical ion release profile from bioactive glass.

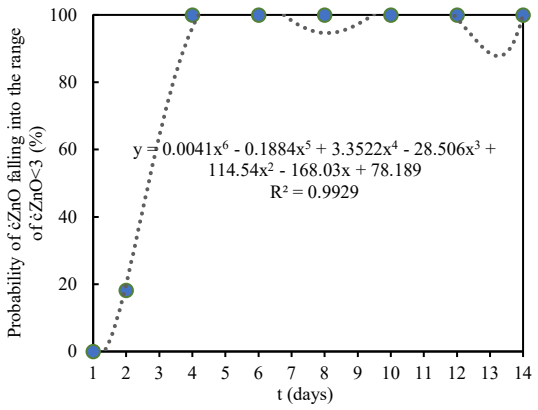

Fig. 4. The success probability of time derivation of ZnO concentration release in terms of time.

4. Conclusion

In this investigation, the effect of silver (Ag^+) and zinc (Zn^{2+}) ions on bioactive glass utilized for dental applications was examined. Utilizing experimental data derived from [41]. The concentration of Ag_2O and ZnO ions utilized in SBF was modeled based on first order kinetics. The model predictions exhibited good agreement with experimental data, with coefficients of variance of 0.95% for Ag and 7% for Zn, when compared to the testing dataset, suggesting the model provided reasonable estimations concerning ion release behavior.

Results indicated that Zn^{2+}, due to its smaller ionic radius, diffuses through the glass matrix more readily, and that Ag^+ ions are released more slowly and remain more effectively retained within the structure. Monte Carlo simulations were performed to consider the probabilistic nature of ion transport, and the probability of different release scenarios; an important consideration for their clinical use. The Monte Carlo simulations revealed Ag_2O sustained release concentrations greater than the therapeutic threshold for approximately 9 days prior to dropping sharply after day 10. Indicating that there should be some antimicrobial effect for the early stages of application. Additionally, ZnO exhibited the rapid, initial release of ions, with the concentration dropping below the therapeutic threshold within the first 5 days, indicating an effect that may facilitate pulp and dentin regeneration during the early, formative stages of regeneration. Overall, this study identifies the importance of ionic size in regulating ion release and describes how to optimize incorporation of Ag^+ and Zn^{2+} to fabricate bioactive dental materials including restorative cements, liners, and coatings for implants.

Author contributions

Masoumeh Khamehchi: Conceptualization, Modeling, Methodology, Investigation, Writing – original draft, Writing – review & editing. **Ana Chkhenkeli:** Writing – original draft, Writing – review & editing.

Funding

No funding was received for this study.

Conflict of interest

The authors declare no conflict of interest.

Data availability

No data is available.

REFERENCES

[1] F. Baino, G. Novajra, V. Miguez-Pacheco, A.R. Boccaccini, C. Vitale-Brovarone, Bioactive glasses: Special applications outside the skeletal system, Journal of Non-Crystalline Solids 432 (2016) 15-30.

[2] Z. Ahmadi, F. Moztarzadeh, Synthesizing and characterizing of gelatin-chitosan-bioactive glass (58s) scaffolds for bone tissue engineering, Silicon 10(4) (2018) 1393-1402.

[3] L. Ji, W. Qiao, K. Huang, Y. Zhang, H. Wu, S. Miao, H. Liu, Y. Dong, A. Zhu, D. Qiu, Synthesis of nanosized 58S bioactive glass particles by a three-dimensional ordered macroporous carbon template, Materials Science and Engineering: C 75 (2017) 590-595.

[4] M.G. Olthof, M.A. Tryfonidou, X. Liu, B. Pouran, B.P. Meij, W.J. Dhert, M.J. Yaszemski, L. Lu, J. Alblas, D.H. Kempen, Phosphate functional groups improve oligo [(polyethylene glycol) fumarate] osteoconduction and BMP-2 osteoinductive efficacy, Tissue Engineering Part A 24(9-10) (2018) 819-829.

[5] G. Rajkumar, V. Dhivya, S. Mahalaxmi, K. Rajkumar, G. Sathishkumar, R. Karpagam, Influence of fluoride for enhancing bioactivity onto phosphate based glasses, Journal of Non-Crystalline Solids 493 (2018) 108-118.

[6] A. Bakhtiari, A. Cheshmi, M. Naeimi, S.M. Fathabad, M. Aliasghari, A.M. Chahardehi, S. Hassani, V. Elhami, Synthesis and characterization of the novel 80S bioactive glass: bioactivity, biocompatibility, cytotoxicity, Journal of Composites and Compounds 2(4) (2020) 110-114.

[7] J. Esmaeilzadeh, S. Hesaraki, S. Borhan, Poly (d/l) lactide-polycaprolactone/bioactive glass nanocomposites: assessments of in vitro bioactivity and biodegradability, Journal of Composites and Compounds 3(9) (2021) 206-212.

[8] S. Bouhazma, S. Chajri, M. Khaldi, M. Sadiki, H. Barkai, S. Elabed, S.I. Koraichi, B. El Bali, M. Lachkar, Characterization in vitro studies and antibacterial properties on a sol-gel derived silver incorporated bioglass, IOP Conference Series: Materials Science and Engineering, IOP Publishing, 2017, p. 012022.

[9] S. Pourshahrestani, N.A. Kadri, E. Zeimaran, N. Gargiulo, S. Samuel, S.V. Naveen, K. Hasikin, T. Kamarul, M.R. Towler, Comparative efficacy of hemorrhage control of a novel mesoporous bioactive glass versus two commercial hemostats, Biomedical Materials 13(2) (2018) 025020.

[10] S. Solgi, M. Khakbiz, M. Shahrezaee, A. Zamanian, M. Tahriri, S. Keshtkari, M. Raz, K. Khoshroo, S. Moghadas, A. Rajabnejad, Synthesis, characterization and in vitro biological evaluation of sol-gel derived Sr-containing nano bioactive glass, Silicon 9(4) (2017) 535-542.

[11] A.A. El-Rashidy, J.A. Roether, L. Harhaus, U. Kneser, A.R. Boccaccini, Regenerating bone with bioactive glass scaffolds: A review of in vivo studies in bone defect models, Acta biomaterialia 62 (2017) 1-28.

[12] W.C. Lepry, S. Smith, S.N. Nazhat, Effect of sodium on bioactive sol-gel-derived borate glasses, Journal of Non-Crystalline Solids 500 (2018) 141-148.

[13] N.N. Ilkhechi, A. Ahmadi, B.K. Kaleji, Optical and structural properties of nanocrystalline anatase powders doped by Zr, Si and Cu at high temperature, Optical and quantum electronics 47(8) (2015) 2423-2434.

[14] H. Ylänen, Bioactive glasses: materials, properties and applications, Woodhead publishing2017.

[15] N. van Gestel, F. Gabriels, B. van Rietbergen, J. Arts, S. Hofmann, Mechanical properties of bioactive glasses, Bioactive Glasses, Elsevier2018, pp. 87-102.

[16] Z. Hong, R.L. Reis, J.F. Mano, Preparation and in vitro characterization of novel bioactive glass ceramic nanoparticles, Journal of Biomedical Materials Research Part A: An Official Journal of The Society for Biomaterials, The Japanese Society for Biomaterials, and The Australian Society for Biomaterials and the Korean Society for Biomaterials 88(2) (2009) 304-313.

[17] A. Abdelghany, H. ElBatal, A. Okasha, R. Ramadan, A. Wassel, A. Menazea, Compatibility and bone bonding efficiency of gamma irradiated Hench's bioglass, Silicon 10(4) (2018) 1533-1541.

[18] A.R. Rouhani, A.H. Esmaeil-Khanian, F. Davar, S. Hasani, The effect of agarose content on the morphology, phase evolution, and magnetic properties of CoFe2O4 nanoparticles prepared by sol-gel autocombustion method, International Journal of Applied Ceramic Technology 15(3) (2018) 758-765.

[19] A.A. El-Rashidy, G. Waly, A. Gad, A.A. Hashem, P. Balasubramanian, S. Kaya, A.R. Boccaccini, I. Sami, Preparation and in vitro characterization of silver-doped bioactive glass nanoparticles fabricated using a sol-gel process and modified Stöber method, Journal of Non-Crystalline Solids 483 (2018) 26-36.

[20] H. Gul, S. Zahid, S. Zahid, M. Kaleem, A.S. Khan, A.T. Shah, Sol-gel derived fluoride-doped bioactive glass powders: Structural and long-term fluoride release/pH analysis, Journal of non-crystalline solids 498 (2018) 216-222.

[21] E. Sharifi Sedeh, S. Mirdamadi, F. Sharifianjazi, M. Tahriri, Synthesis and evaluation of mechanical and biological properties of scaffold prepared from Ti and Mg with different volume percent, Synthesis and Reactivity in Inorganic, Metal-Organic, and Nano-Metal Chemistry 45(7) (2015) 1087-1091.

[22] A. Balamurugan, G. Balossier, D. Laurent-Maquin, S. Pina, A. Rebelo, J. Faure, J. Ferreira, An in vitro biological and anti-bacterial study on a sol–gel derived silver-incorporated bioglass system, dental materials 24(10) (2008) 1343-1351.

[23] Y. Weng, H. Liu, S. Ji, Q. Huang, H. Wu, Z. Li, Z. Wu, H. Wang, L. Tong, R.K. Fu, A promising orthopedic implant material with enhanced osteogenic and antibacterial activity: Al2O3-coated aluminum alloy, Applied Surface Science 457 (2018) 1025-1034.

[24] F. Sharifianjazi, N. Parvin, M. Tahriri, Formation of apatite nano-needles on novel gel derived SiO2-P2O5-CaO-SrO-Ag2O bioactive glasses, Ceramics International 43(17) (2017) 15214-15220.

[25] W. Wu, W. Zhao, Y. Wu, C. Zhou, L. Li, Z. Liu, J. Dong, K. Zhou, Antibacterial behaviors of Cu2O particles with controllable morphologies in acrylic coatings, Applied Surface Science 465 (2019) 279-287.

[26] K. Ghazal, S. Shoaib, M. Khan, S. Khan, M.K. Rauf, N. Khan, A. Badshah, M.N. Tahir, I. Ali, Synthesis, characterization, X-ray diffraction study, in-vitro cytotoxicity, antibacterial and antifungal activities of nickel (II) and copper (II) complexes with acyl thiourea ligand, Journal of Molecular Structure 1177 (2019) 124-130.

[27] J. Liu, S.C. Rawlinson, R.G. Hill, F. Fortune, Fluoride incorporation in high phosphate containing bioactive glasses and in vitro osteogenic, angiogenic and antibacterial effects, dental materials 32(10) (2016) e221-e237.

[28] F. Sharifianjazi, N. Parvin, M. Tahriri, Synthesis and characteristics of sol-gel bioactive SiO2-P2O5-CaO-Ag2O glasses, Journal of Non-Crystalline Solids 476 (2017) 108-113.

[29] M. Eltohamy, B. Kundu, J. Moon, H.-Y. Lee, H.-W. Kim, Anti-bacterial zinc-doped calcium silicate cements: bone filler, Ceramics International 44(11) (2018) 13031-13038.

[30] J.S. Fernandes, P. Gentile, R.A. Pires, R.L. Reis, P.V. Hatton, Multifunctional bioactive glass and glass-ceramic biomaterials with antibacterial properties for repair and regeneration of bone tissue, Acta biomaterialia 59 (2017) 2-11.

[31] J.-C. Kung, Y.-J. Chen, Y.-C. Chiang, C.-L. Lee, Y.-T. Yang-Wang, C.-C. Hung, C.-J. Shih, Antibacterial activity of silver nanoparticle (AgNP) confined mesoporous structured bioactive powder against Enterococcus faecalis infecting root canal systems, Journal of Non-Crystalline Solids 502 (2018) 62-70.

[32] A.C. Vale, A.L. Carvalho, A.M. Barbosa, E. Torrado, J.F. Mano, N.M. Alves, Novel antibacterial and bioactive silicate glass nanoparticles for biomedical applications, Advanced Engineering Materials 20(5) (2018) 1700855.

[33] N. Najibi Ilkhechi, M.R. Akbarpour, R. Yavari, Z. Azar, Sn4+ and La3+ co doped TiO2 nanoparticles and their optical, photocatalytic and antibacterial properties under visible light, Journal of Materials Science: Materials in Electronics 28(22) (2017) 16658-16664.

[34] R. Phetnin, S.T. Rattanachan, Preparation and antibacterial property on silver incorporated mesoporous bioactive glass microspheres, Journal of Sol-Gel Science and Technology 75(2) (2015) 279-290.

[35] R. Zeeshan, Z. Mutahir, H. Iqbal, M. Ali, F. Iqbal, K. Ijaz, F. Sharif, A.T. Shah, A.A. Chaudhry, M. Yar, Hydroxypropylmethyl cellulose (HPMC) crosslinked chitosan (CH) based scaffolds containing bioactive glass (BG) and zinc oxide (ZnO) for alveolar bone repair, Carbohydrate polymers 193 (2018) 9-18.

[36] V.P.S. Sidhu, R. Borges, M. Yusuf, S. Mahmoudi, S.F. Ghorbani, M. Hosseinikia, P. Salahshour, F. Sadeghi, M. Arefian, A comprehensive review of bioactive glass: synthesis, ion substitution, application, challenges, and future perspectives, Journal of Composites and Compounds 3(9) (2021) 247-261.

[37] A.M. El-Kady, A.F. Ali, Fabrication and characterization of ZnO modified bioactive glass nanoparticles, Ceramics International 38(2) (2012) 1195-1204.

[38] M. Raz, F. Moztarzadeh, S.S. Kordestani, Sol-gel based fabrication and properties of Mg-Zn doped bioactive glass/gelatin composite scaffold for bone tissue engineering, Silicon 10(2) (2018) 667-674.

[39] J. Rivadeneira, A. Gorustovich, Bioactive glasses as delivery systems for antimicrobial agents, Journal of Applied Microbiology 122(6) (2017) 1424-1437.

[40] M. Akram, R. Hussain, Antibacterial properties of bioactive glasses, Clinical Applications of Biomaterials: State-of-the-Art Progress, Trends, and Novel Approaches, Springer2017, pp. 357-382.

[41] M.S.N. Shahrbabak, F. Sharifianjazi, D. Rahban, A. Salimi, A comparative investigation on bioactivity and antibacterial properties of sol-gel derived 58S bioactive glass substituted by Ag and Zn, Silicon 11(6) (2019) 2741-2751.

[42] J. Zou, Y. Xu, B. Hou, D. Wu, Y. Sun, Controlled growth of silver nanoparticles in a hydrothermal process, China Particuology 5(3) (2007) 206-212.
[43] V.F. Alencar, J.C. Oliveira, A.S. Pereira, S.M. Lucena, Molecular simulation and machine learning tools to predict bioglass modulus of elasticity, Journal of Non-Crystalline Solids 618 (2023) 122507.
[44] H. Chen, Q. Shi, K. Zheng, Mathematical modeling of bioactive glass degradation, Journal of Non-Crystalline Solids 646 (2024) 123265.
[45] M. Mahmoodi, M. Khamehchi, Random distribution of interphase characteristics on the overall electro-mechanical properties of CNT piezo nanocomposite: Micromechanical modeling and Monte Carlo simulation, Probabilistic Engineering Mechanics 75 (2024) 103577.